ELSEVIER

Journal of Chromatography A, 905 (2001) 19–34

JOURNAL OF CHROMATOGRAPHY A

www.elsevier.com/locate/chroma

Nuclear magnetic resonance studies of solvent flow through chromatographic columns: effect of packing density on flow patterns

Sally G. Harding[a,*], Herbert Baumann[b]

[a]*Department of Chemistry, Swedish University of Agricultural Sciences, Arrheniusplan 8, P.O. Box 7015, SE 750 07 Uppsala, Sweden*
[b]*Amersham Pharmacia Biotech AB, SE 751 84 Uppsala, Sweden*

Received 4 April 2000; received in revised form 29 August 2000; accepted 18 September 2000

Abstract

NMR (nuclear magnetic resonance) techniques have been used to measure and characterise solvent flow through chromatographic columns. NMR imaging was used to track an injection of D_2O. PGSE (pulsed gradient spin echo) NMR was used to measure the flow-rate dependence of axial and transverse apparent diffusion. A combination of these two techniques (dynamic NMR imaging) gave the spatial distribution of the local velocity and apparent diffusion through a cross-section of the column. Significant column wall effects were observed and these effects were found to be highly dependent upon the column packing density. The column performance was assessed in terms of the HETP (height equivalent to a theoretical plate) determined by the NMR techniques employed.

Keywords: Diffusion; Packing density; Flow rate; Pulsed gradient spin echo; Nuclear magnetic resonance spectrometry

1. Introduction

The aim of this work was to evaluate the potential of nuclear magnetic resonance (NMR) techniques employing magnetic field gradients to give information about the flow characteristics of the mobile phase in chromatographic columns. Experimental techniques which provide insights into zone broadening, diffusion and the velocity distribution through a column are desired to relate the underlying transport behaviour of the solvent flow to the overall macroscopic column performance. This knowledge can then be used to improve the rational evaluation and development of new column designs and packing techniques.

Column efficiency is determined by the broadening of a band or zone as it moves through a column and is quantified in terms of height equivalent to a theoretical plate, HETP. The HETP, H, is defined as the slope of the dependence of the zone variance, σ^2, on its migration distance, z [1]. The reduced HETP, h is defined as:

$$h = \frac{H}{d_p} = \frac{1}{d_p}\frac{\partial \sigma^2}{\partial z} \quad (1)$$

where d_p is the average particle diameter. Empirical relationships such as those suggested by van Deem-

*Corresponding author. Tel.: +46-18-671-553; fax: +46-18-673-477.

E-mail address: Sally.Harding@kemi.slu.se (S.G. Harding).

0021-9673/01/$ – see front matter
PII: S0021-9673(00)00968-7

ter and Knox have frequently been used to describe the relationship between the reduced plate height and the mobile phase velocity [2]. In such relationships the mobile phase velocity is expressed as a reduced velocity, v, of the inter particle fluid:

$$v = \frac{ud_p}{D_m} \tag{2}$$

where u is the cross-sectional average velocity of the inter particle fluid and D_m the diffusion coefficient of the free liquid. Knox [2] suggested that the axial reduced plate height h_a is related to the reduced velocity by the expression:

$$h_a = \frac{B}{v} + Av^n + Cv \tag{3}$$

where A, B, C are numerical coefficients characterising the packed bed and eddy diffusion, axial diffusion and mass transfer resistance respectively and n is typically taken to be $1/3$. In the transverse direction the analogous expression is:

$$h_t = \frac{B}{v} + D \tag{4}$$

where D is a coefficient accounting for the contribution of eddy diffusion to radial dispersion.

Evidence in support of the heterogeneous nature of the packing of chromatography columns has recently been reviewed [3]. Giddings [1] described the various mechanisms that can lead to fluctuations in the local mobile phase velocity across a column. He divided these contributions into five groups in order of increasing length scale: trans particle, trans channel, short range inter channel, long range inter channel and trans column contributions. The relative importance of these different contributions is however poorly examined.

NMR techniques using magnetic field gradients are attracting considerable attention as probes of porous materials. The measurements are non-destructive and do not have to involve the introduction of chemical tracers. NMR techniques have been extensively applied to the study of packed or consolidated beds of impermeable particles or beads [4], however less research has concentrated on columns packed with porous particles, such as the gels used in chromatography applications. Details of the NMR techniques employed can be found elsewhere [5].

NMR imaging offers considerable potential for monitoring in real time the migration and dispersion of bands in chromatographic columns. This application of NMR imaging has been demonstrated by several groups [6–13]. These workers have utilised the enhanced solvent T_1 and T_2 relaxation in the presence of paramagnetic tracer ions (gadolinium or manganese) as contrast to selectively image the migrating bands. Significant distortion of the bands has been observed at the column inlets and as a result of packing irregularities and the effects of viscous fingering has been monitored. Concentration profiles of tracers in chromatographic columns have been used to determine local and average column HETP values [11].

Pulsed Gradient Spin Echo (PGSE) NMR has been used to measure the solvent axial and transverse apparent diffusion coefficients averaged over a large section of the column over an experimentally adjustable observation time [14–16]. From these results the dependence of the axial and transverse HETP on the fluid velocity has been measured. PGSE experiments have also been analysed in terms of the dynamic displacement profile to distinguish non-flowing (stagnant) solvent within the porous particles from the solvent flowing around the particles. Thus it has been possible to follow the mass transfer between the stagnant solvent and the stream percolating through the column bed [17–21].

By combining the PGSE technique with NMR imaging it is possible to measure the flow velocity and apparent diffusion coefficient with spatial resolution — thus local variations in flow velocity and apparent diffusion can be directly monitored. This technique has been used to study solvent flow through packed columns of impermeable beads [4,22–27]. Recently the potential of the technique to study the spatial distribution of velocity and apparent diffusion in chromatographic columns has been demonstrated [28,29]. These studies found that spherically shaped particles showed a uniform velocity across the column cross-section, while larger, irregular shaped particles showed evidence of external porosity heterogeneities which accounted for a dramatic loss in performance. Both columns were radially compressed and no edge effects were seen in either system.

In this current study three different NMR tech-

niques that can be used to monitor solvent flow through chromatographic columns are employed; NMR imaging, PGSE NMR and dynamic NMR imaging. All three experimental techniques measure the effect of zone broadening and mobile phase flow fluctuations over different length and time scales and thus allow the varying contributions of these effects on the overall column performance to be assessed. NMR imaging is used to track the progression of an injection of deuterated water (D_2O) as it moves through the column. This experiment therefore measures the effect of column inlet and directly visualises the solvent zone broadening through the column. PGSE NMR is used to measure axial and transverse apparent diffusion coefficients averaged over a large portion of the column and measured over a well defined observation time (typically 200 ms). This technique is therefore sensitive to trans particle, trans channel and inter channel velocity fluctuations. Dynamic NMR imaging is used to measure the spatial distribution of solvent velocity and across the column. The dynamic NMR imaging experiment can therefore measure trans column flow fluctuations. These experiments have been used to asses the effect of column packing density on the observed solvent flow characteristics.

1.1. Dynamic NMR methods

The following summary will briefly describe the essential principles of the PGSE NMR technique thought necessary for the comprehension of the presented results. More detailed reviews can be found elsewhere [4,5]. In summary, PGSE NMR monitors the motion of molecules over an observation time, Δ, between successive motion encoding pulses of magnetic field gradient. The direction of the applied gradient pulses will determine the direction in which the motion is measured. The strength, g, and duration, δ, of the motion encoding gradient pulses are described by the wave vector $\boldsymbol{q}$, where $\boldsymbol{q}$ is defined as $\boldsymbol{q} = 1/2\pi\ \gamma\delta g$. The signal attenuation $S(\boldsymbol{q},\Delta)$ is then given by:

$$S(\boldsymbol{q},\Delta) = \int \bar{P}_s(\boldsymbol{R},\Delta) \exp[i2\pi\boldsymbol{q}.\boldsymbol{R}]\, \mathrm{d}\boldsymbol{R} \tag{5}$$

where $\bar{P}_s(\boldsymbol{R},\Delta)$ is the average probability for the observed molecule to have a dynamic displacement, $\boldsymbol{R}$, over the time interval Δ — often referred to as the dynamic displacement profile. Thus the signal intensity is related via Fourier transformation to the dynamic displacement profile. If the motion can be described by an apparent diffusion coefficient, D_{app}, and a mean velocity, $\bar{u}$, the signal attenuation will then be:

$$S(\mathbf{q}) = \exp(i2\pi\mathbf{q}\bar{u}) \exp\left(-4\pi^2\boldsymbol{q}^2 D_{\mathrm{app}}\left(\Delta - \frac{\delta}{3}\right)\right). \tag{6}$$

The signal attenuation is therefore described by an oscillatory term determined by the velocity and a decaying term determined by the apparent diffusion coefficient. The dynamic displacement profile has a gaussian distribution, centred at $\bar{u}\Delta$ in the displacement space and a standard deviation of $(2D_{\mathrm{app}}\Delta)^{1/2}$. Thus under these conditions the apparent diffusion and velocity can be obtained from the width and peak centre of the profile respectively. The HETP, H_{PGSE}, and reduced HETP, h_{PGSE} determined from the PGSE apparent diffusion coefficient, is given by [14–16]:

$$H_{\mathrm{PGSE}} = \frac{2D_{\mathrm{app}}}{\bar{u}}, \quad h_{\mathrm{PGSE}} = \frac{2D_{\mathrm{app}}}{\bar{v}D_m} \tag{7}$$

This equation is derived from Giddings [1] definition of the HETP and the classical definition of the diffusion constant. D_m is the diffusion coefficient in the bulk mobile phase and $\bar{u}$ and $\bar{v}$ are the velocity and reduced velocity averaged over the observation time, Δ, and are distinct from u and v which correspond to the velocity of the inter particle fluid.

2. Experimental

2.1. Materials

Two types of chromatography systems have been investigated; Amersham Pharmacia Biotech HiTrap Phenyl Sepharose High Performance 1 ml, a hydrophobic interaction chromatography (HIC) separation column and solid-phase extraction (SPE) columns manually packed to three different packing densities. Both the HiTrap and SPE columns were made from

polypropylene. The packing material used in both the HiTrap and SPE columns was an agarose based Sepharose High Performance gel — a spherical highly cross linked agarose (6%) with a particle diameter of 34±10 μm. The 1 ml HiTrap columns have 25 μmol ml^{-1} gel hydrophobic phenyl ligand residues linked to the hydrophilic base matrix. The HiTrap columns have an internal diameter of 7 mm and a length of 25 mm. The SPE columns have an internal diameter of 5.8 mm and were prepared with varying degrees of column compression as described in Table 1. The solid-phase and inter particle fraction of the three prepared columns are also shown in Table 1 and have been calculated from the solid-phase fraction (0.06) and intra particle void fraction (0.3) [30] of the original gel material. The data reported in Table 1 refers to the columns as manufactured. The SPE column packed with the lowest packing density 'column A', however, was further compressed by the flow of water through the column during column conditioning prior to the start of the NMR experiments. The data reported in Table 1 for 'column A' gives the lower limit of the packing density of this column but it should be noted that consolidation of the bed as a result of the water flow will act to reduce the inter particle void fraction slightly. To test the reproducibility of the columns, two 1 ml HiTrap columns and two SPE columns (column A) were studied. De-ionised de-gassed water was pumped through the columns using a dual syringe pump. Approximately 3 m of liquid chromatography (LC) Teflon tubing was used to allow the pump to be positioned a safe distance from the magnet. Before the start of the NMR measurements water was pumped through the column at a flow-rate of 2 ml min^{-1} (HiTrap column) or 1 ml min^{-1} (SPE columns) for 1 h to minimise any further packing rearrangements occurring during the time course of the experiment. The construction of the SPE columns requires that there has to be a reservoir of water on top of the bed as shown schematically in Fig. 1b.

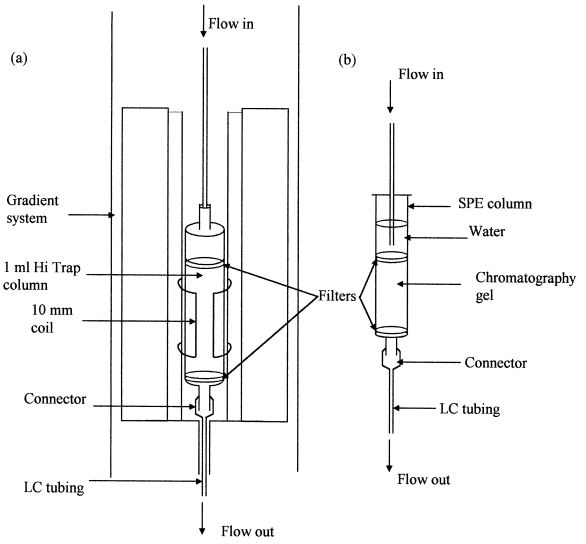

Fig. 1. (a) Schematic representation of the configuration of the NMR instrument for measurements on chromatographic columns showing the 1 ml HiTrap column. (b) Schematic view of the SPE column.

2.2. NMR measurements

The NMR measurements were carried out using a Bruker DMX 600 NMR spectrometer equipped with a micro-imaging accessory and a 10 mm coil. The thermocouple and heating element was removed from the probe to allow the LC tubing to be run vertically through the magnet. The experimental set-up is outlined in Fig. 1. The column axis is parallel to the main magnetic field and unless otherwise stated the column was centred vertically within the coil, so the middle portion of the column was in the

Table 1
Description of the solid-phase extraction (SPE) columns prepared with different packing densities

Column	Volume gel (μl)	Column height (mm)	Column compression (volume gel/column height) (μl mm^{-1})	Inter particle void fraction	Solid phase fraction
A	400	22	18.2	0.51	0.042
B	500	22	22.7	0.39	0.053
C	500	20	25.0	0.32	0.058

active field of view. Standard LC fittings and connectors were used, in some cases the outer edges of the connectors had to be cut away to allow the columns to fit into the 10 mm coil. The spectral line-width of the water was around 50 Hz.

2.3. NMR imaging of D_2O injection

D_2O is invisible in a proton NMR image, so by monitoring the loss in signal intensity due to the replacement of H_2O by D_2O it is possible to follow the progression of an injection of D_2O as it passes through the column. H_2O was pumped through the column at a flow-rate of 0.5 ml min^{-1} and a 100 μl sample of D_2O was injected into the system whilst maintaining a constant flow-rate. A series of 32 images were then acquired using a gradient echo sequence with a low flip angle and fast repetition time (FLASH — Fast Low Angle SHot). The image slices were aligned vertically, with the read direction parallel to the flow direction. The imaging slice was 1 mm thick and contained 256×128 pixels covering a field of view of 20×10 mm. The repetition time was 18.63 ms, two scans were co-added, giving a total acquisition time of 4.77 s for each image. Images were acquired every 5.24 s. The experiment was repeated with varying portions of the column positioned within the active field of view, thus allowing the top, middle and lower portions of the column to be imaged in turn. The images were acquired within a 3D data set to save time writing the data to disk during the fast acquisitions. The data was transferred to MATLAB for further processing. All subsequent images were subtracted from the first image, and then divided by the first image so that the loss in intensity due to the presence of D_2O could be visualised.

2.4. PGSE measurements

PGSE measurements were made using the stimulated echo PGSE sequence [5]. To allow additional verification of the motional regime, some measurements were also carried out using an double PGSE technique [4] in which the sense of phase shift for displacement is opposite in the successive gradient pulse pairs. In each experiment the gradient amplitude was incremented in 32 steps while the gradient duration, δ, and gradient separation, Δ, were kept constant. The experiments were carried out using Δ values of between 20 and 400 ms. The experiments were repeated at flow-rates up to 2 ml min^{-1} for the HiTrap™ column and up to 1 ml min^{-1} for the SPE columns. The apparent diffusion coefficient, D_{app}, was calculated by fitting the equation:

$$|S(\boldsymbol{q})| = \exp\left(-4\pi^2 \boldsymbol{q}^2 D_{app}\left(\Delta - \frac{\delta}{3}\right)\right) \quad (8)$$

to the modulus of the signal intensity in the low $\boldsymbol{q}$ limit (defined by $4\pi^2\boldsymbol{q}^2\Delta D_{app} < 1$). By application of gradient pulses parallel and perpendicular to the main flow direction, the apparent diffusion, D_{app}, and reduced plate height, h_{PGSE}, in both axial and transverse directions were measured.

2.5. Dynamic NMR imaging

Velocity and apparent diffusion images were measured using a phase encoding method described in detail elsewhere [5]. The pulse sequence used consisted of a stimulated echo PGSE sequence as preconditioning to a standard spin echo image sequence. The velocity and apparent diffusion maps were obtained by acquiring 8–16 images in which the magnetic field gradient, g, used to encode for motion is successively stepped in magnitude, in n_D intervals, up to a maximum value g_m. Typically, the flow gradient duration, δ, was 0.5 ms, the maximum gradient strength, g_m, was 25 G cm^{-1} and the gradient separation time, Δ, was 200 ms. Two dimensional (2D) dynamic images were acquired perpendicular to the main flow direction across the column cross-section and the motion encoding gradients were applied parallel to the main flow direction to allow measurement of axial velocity and apparent diffusion. The imaging slice thickness was 1 mm and the in plane resolution was 39.0μm/pixel (1 ml HiTrap™ columns) or 46.9 μm/pixel (SPE columns).

The dynamic imaging data sets were Fourier transformed in the two spatial dimensions and the flow dimension to provide the dynamic displacement profile for the motion in each pixel of the image. Prior to Fourier transformation in the flow direction the data was zero filled to give N (typically 128) data

points in the dynamic displacement profile. The data was then transferred to MATLAB for further processing. A gaussian distribution was fitted to the dynamic displacement profile for each pixel in the image. The peak position, k_v, and full width half maximum, k_{FWHM}, determined from the fitting procedure was then used to calculate the flow velocity, $\bar{u}$, and the apparent diffusion, D_{app}, at each point in the image using Eqs. (9) and (10) respectively.

$$\bar{u} = \frac{2\pi n_D k_v}{N\gamma\delta\Delta g_m} \quad (9)$$

$$D = \frac{3.56(n_D k_{FWHM})^2}{\gamma^2\delta^2 g_m^2 N\Delta} \quad (10)$$

In this way maps of the local velocity and local apparent diffusion coefficient were constructed. Radial averaged profiles of velocity and dispersion were calculated from the 2D images by averaging pixels within a specified radial interval from the centre of the image, for all such radial intervals. The '*x*–*y*' co-ordinates of the centre of the image was determined from the total intensity image by fitting the projections of the image in the *x* and *y* directions to equations for the projection of a circle onto a line.

3. Results and discussion

3.1. NMR imaging of D_2O injection

Typical images of the flow of a 100 μl injection of D_2O through the column are shown in Fig. 2. The images were acquired when the column was positioned so that the inlet of the column was within the imaging active region. This set-up allows the effect of the column inlet on the band broadening to be studied. The upwards curvature of the band towards the edge of the column is clearly a conse-

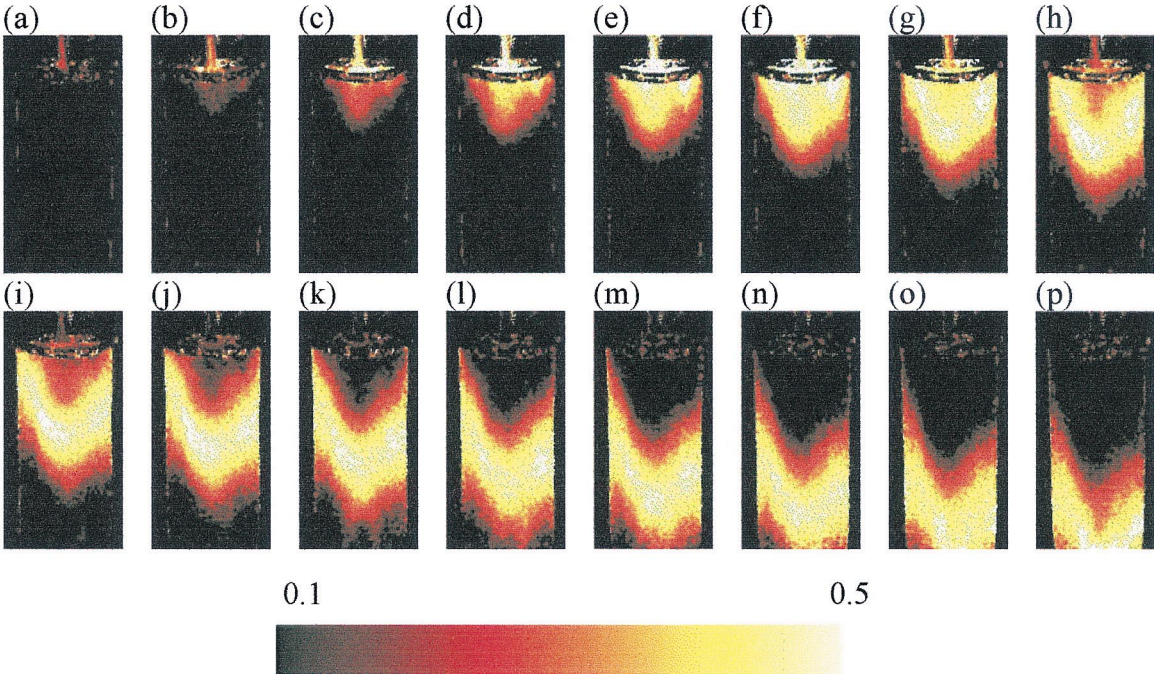

Fig. 2. NMR images of an injection of D_2O passing through the 1 ml HiTrap™ column operating at a flow-rate of 0.5 ml min^{-1}. The images are orientated along the axis of the column, with the column inlet at the top. The images are calculated by subtraction from the first image acquired before the D_2O had entered the column. The intensity scale shows the fractional loss in signal intensity relative to the first image. The images (a)–(p) were acquired at intervals of 5.24 s. The field of view of the displayed images is 9.38 mm in the horizontal direction and 18.75 mm in the vertical direction.

quence of the commonly used inlet design. The injected sample takes a longer time to travel to the outer region of the column and thus lags behind the sample that flows into the central region of the column. This band curvature remained apparent as the D_2O injection moved along the complete length of the column. The results shown in Fig. 2 show distinct similarities with those obtained by direct optical visualisation [31–35].

The ability to image the progression of the D_2O band through the column should allow the change in the band variance of the D_2O sample as it moves through the column to be measured so allowing the HETP to be determined. This proved to be rather difficult, due to the high diffusivity of water (much higher than most compounds that would be separated in the column). Significant mixing of the D_2O sample with H_2O occurs in the LC tubing and in the column inlet filter. This dilutes and broadens the band significantly before it has entered the main body of the column and so limits the number of images when the complete band is within the imaging region and makes it difficult to image a smaller injection volume. The band broadening as the sample passes through the field of view was small relative to the imaging resolution. The band variance was estimated by fitting a gaussian distribution to the D_2O profile and was found to increase by only approximately 100 μm^2 as the centre of the band moved by 4 mm — equating to a reduced HETP of around 0.7. Although this method does not allow the HETP to be accurately determined it allows some comparison with the HETP determined from the PGSE diffusion measurements and velocity images. It can clearly be seen that the band broadening induced by flow of the band through the main body of the column is minimal compared to the band broadening induced by the column inlet.

3.2. PGSE measurements

Analysis of the PGSE measurements (acquired with no spatial resolution) describe the properties of the fluid flow averaged over a large section of the column. Fig. 3(a),(b), and (c) show different representations of the data obtained from PGSE experiments. The data shown in Fig. 3 is for the 1 ml HiTrap™ column, however similar trends were also seen for the SPE columns. Fig. 3(a) shows dynamic displacement profiles for a flow-rate of 1 ml min^{-1} measured parallel to the flow direction over observation times of 20 and 400 ms. For short observation times, Δ, the dynamic displacement profiles are asymmetric due to partial separation of peaks corresponding to the mobile inter particle and stagnant intra particle liquid. For longer times, however, the profiles become more gaussian in character due to mixing of the intra and inter particle water. This trend can be seen in Fig. 3(a) by comparing the dynamic displacement profiles to the fit of a gaussian distribution to the data. Fig. 3(b) shows representative plots of the modulus of the signal, $\ln(|S|)$, as a function of the fit parameter $4\pi^2 q^2 D_{app}(\Delta - \delta/3)$ — according to the form of Eq. (8). The data is shown for a flow-rate of 2 ml min^{-1} at varying observation times, Δ, again with the gradient orientated parallel to the flow direction. Deviation from the linear decay of $\ln(|S|)$ with $\boldsymbol{q}^2$, as $\boldsymbol{q}$ increases is evident for each set of data acquired with a constant Δ value. This deviation becomes less significant as the observation time, Δ, is increased. In the low $\boldsymbol{q}$ limit — defined as $4\pi^2 q^2 \Delta D_{ap} < 1$, the signal attenuation, $\ln(|S|)$, is linear with $\boldsymbol{q}^2$, and can be used to calculate the apparent diffusion by fitting to Eq. (8) [4]. Determination of the apparent diffusion from the low $\boldsymbol{q}$ limit linear decay shows that there is a slight but significant increase in the apparent diffusion with increasing observation time, Δ. This is further highlighted in Fig. 3(c) which shows that the measured apparent diffusion increases when Δ is increased from 20 to 200 ms, but then appears to reach an asymptotic value at Δ values greater than or equal to 200 ms. The trends seen in Fig. 3(a)–(c)with increasing observation time, Δ, can be rationalised by considering the mean distance moved over the observation time, Δ, relative to the mean particle diameter and pore size. In the short observation time limit the mean distance moved ($\bar{u}\Delta$) is small in comparison to the particle diameter ($\bar{u}\Delta < d_p$) and there is incomplete averaging of the inter and intra particle fluid and pore scale inhomogeneities. In this regime the dynamic displacement profile is asymmetric, the modulus of the signal is incompletely described by a single diffusion coefficient [Eq. (8)], and the apparent diffusion coefficient determined from the low $\boldsymbol{q}$ limit attenuation is a function of the

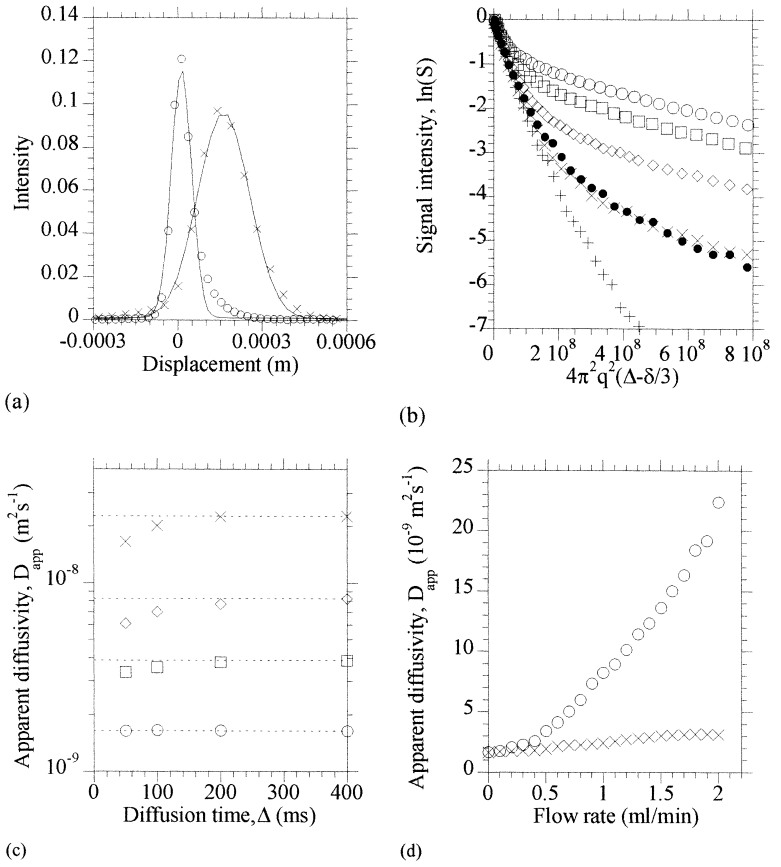

Fig. 3. PGSE measurements for the 1 ml HiTrap™ column. (a) Dynamic displacement profiles acquired parallel to the flow direction at a flow-rate of 1 ml min^{-1} and measured over observation times, Δ, of: (—○) 20 ms and (—×) 400 ms. The solid line (—) show the fitted gaussian distributions. (b) Modulus of the NMR signal, ln(|S|), as a function of $4\pi^2q^2(\Delta-\delta/3)$ for a flow-rate of 2 ml min^{-1}, measured parallel to the flow direction. Data is shown for observation times, Δ, of (○) 20 ms, (□) 50 ms, (◇) 100 ms, (×) 200 ms and (+) 400 ms, and (●) for the double PGSE with an observation times, Δ, of 200 ms. (c) Apparent diffusion coefficient, D_{app}, measured parallel to the flow direction as a function of observation time, Δ, for flow velocities of (○) 0 ml min^{-1}, (□) 0.5 ml min^{-1}, (◇) 1 ml min^{-1} and (×) 2 ml min^{-1}. The dashed lines (· · · · · ·) represent the asymptotic limit of the apparent diffusion at long Δ times. (d) Apparent diffusion coefficient, D_{app}, as a function of flow-rate, when the diffusion gradients are applied (×) parallel to the flow direction (axial apparent diffusion) and (○) perpendicular to the flow direction time (transverse apparent diffusion).

observation time. As the observation time is increased such that the mean distance moved by the fluid is greater than the particle diameter, $\bar{u}\Delta \gg d_p$, mixing of the inter and intra particle fluid can occur and pore scale inhomogeneities are averaged, so the correlation between the initial and starting liquid positions will be removed. The dynamic displacement profile therefore assumes a gaussian distribution, the modulus of the signal attenuation can be described by a single diffusion coefficient, and the apparent diffusion coefficient becomes independent of the observation time. Analysis of the PGSE data acquired with varying observation time, Δ, implies that using an observation time of around 200 ms fulfils the requirements $\bar{u}\Delta \gg d_p$. This result is supported by making some simple calculations; in 200 ms the root mean squared displacement of the water molecules, assuming a diffusivity of $2\cdot10^{-9}$ m^2 s^{-1} will be approximately 50 μm (larger than the particle diameter) and for a flow-rate 2 ml min^{-1} the average displacement in the flow direction will be of the order of 5 particle diameters.

When measuring the apparent diffusion coefficient from the PGSE data it is very important to be aware of the variation in the apparent diffusion coefficient with observation time Δ. It is therefore important to either take into account the variation of the determined apparent diffusion coefficient with increasing Δ values or to chose a Δ value that is sufficiently large that the apparent diffusion can be assumed to have reached its asymptotic value. For this reason an observation time Δ of 200 ms was used to assess the variation of the apparent diffusion with flow-rate and in the subsequent dynamic imaging experiments. Using a larger Δ value also allows a greater degree of signal attenuation within the low $\boldsymbol{q}$ limit restriction. The value of Δ used in this work is higher than that used in some previous bulk and dynamic imaging studies (30–80 ms) [14,21] but comparable to the value of 150 ms also previously used [16].

To confirm that the use of an observation time Δ of 200 ms leads to the determination of the asymptotic diffusion coefficient the double PGSE sequence [4] was applied at varying flow-rates. Comparison of the signal attenuation data obtained for single and double PGSE sequences showed good agreement, see for example the data shown in Fig. 3(b), comparing the attenuation for single and double PGSE sequences with an observation time Δ of 200 ms. The signal attenuation over the total observation time Δ is the same whether a single or double PGSE pair is used to determined the apparent diffusion. This indicates that the displacements are uncorrelated between each pulse pair, so the variance in the phase spread, leading to signal attenuation is not being refocused by the second pulse pair. This supports the assumption that by utilising an observation time of 200 ms the apparent diffusion determined is in the asymptotic diffusion regime, and is thus independent of the observation time Δ and can be considered a universal parameter.

From the displacement profiles acquired even with the shortest observation time studied it is not possible to distinguish stagnant intra particle and flowing inter particle fluid in contrast to the results reported in related studies [17–21]. This is due to a combination of small particle diameter (34 μm) resulting in substantial exchange of intra and inter particle liquid within the shortest observation times employed (20 ms) and low flow-rate resulting in significant overlap of the peaks from intra and inter particle liquid.

Using an observation time, Δ, of 200 ms the apparent diffusion was determined at varying flow-rates. The variation of the apparent diffusion measured with the gradients oriented in the direction of flow (axial apparent diffusion) and perpendicular to the flow direction (transverse apparent diffusion) with flow-rate is shown in Fig. 3(d). Both axial and transverse apparent diffusion increase with increasing flow-rate, the axial apparent diffusion coefficient, however, increases much more significantly. The reduced plate height, h_{PGSE}, representing the contribution of dispersion over a 200 ms time interval to the overall HETP can be calculated from the PGSE apparent diffusion coefficient [Eq. (7)]. Fig. 4 shows

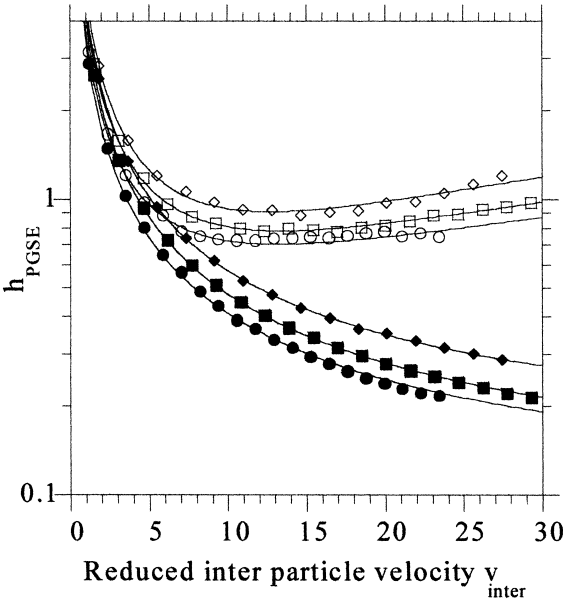

Fig. 4. The axial and transverse reduced plate heights, h_{PGSE} determined from the PGSE apparent diffusion measurements as a function of the reduced inter particle velocity for SPE columns. The data are shown for axial (open symbols) and transverse (filled symbols) h_{PGSE} for columns A (○), (●), B (□), (■) and C (◇), (♦). The solid lines show the fits of Eqs. (3) and (4) to the data for axial and transverse h_{PGSE} respectively, assuming $n=1/3$. The fitted values of the coefficients A, B_{axial} ($H_{\mathrm{transverse}}$), C and D are, respectively: column A — 0.11±0.01, 3.52 ±0.03, (3.3±0.1), 0.014±0.002; 0.082±0.002 column B — 0.09±0.01, 4.22±0.02, (3.92±0.03), 0.018±0.001 0.080±0.002; column C — 0.084±0.02, 4.92±0.08, (4.46±0.005), 0.025±0.003 0.126±0.003.

the variation of h_{PGSE} measured parallel and perpendicular to the main flow with the inter particle velocity for the three SPE columns studied. Plotted in this way the h_{PGSE} value at a given reduced inter particle velocity increases with increasing packing density due to the more tortuous path the flowing inter particle liquid is forced to take. The Knox equation used to describe the variation of the overall reduced plate height with the inter particle velocity could also be fitted to the variation of h_{PGSE} with the inter particle velocity, as shown in Fig. 4. It should be noted that these equations are normally used to model the effect of the flow velocity on the overall plate height determined by chromatography. In this case we find that the same empirical equations can be used to express the relationship between the contribution to the plate height of dispersion over 200 ms (determined by the PGSE experiments) and the solvent velocity.

3.3. Dynamic NMR imaging

Fig. 5 shows typical dynamic displacement profiles acquired at a spatially localised position in the dynamic NMR images. The data shown in Fig. 5 is extracted from two individual pixels; one at the outer edge of the column, where the velocity is higher than average and the other from the middle of the column where the velocity is close to average. The dynamic displacement profiles show approximately a gaussian shape, and the fit of a gaussian distribution to the data is also shown in Fig. 5. The gaussian shape of the dynamic displacement profiles is characteristic of the situation where the mean distance moved by the water is greater than the particle diameter, $\bar{u}\Delta \gg d_p$ so the correlation between the initial and starting liquid positions is removed (as discussed in detail in the previous section).

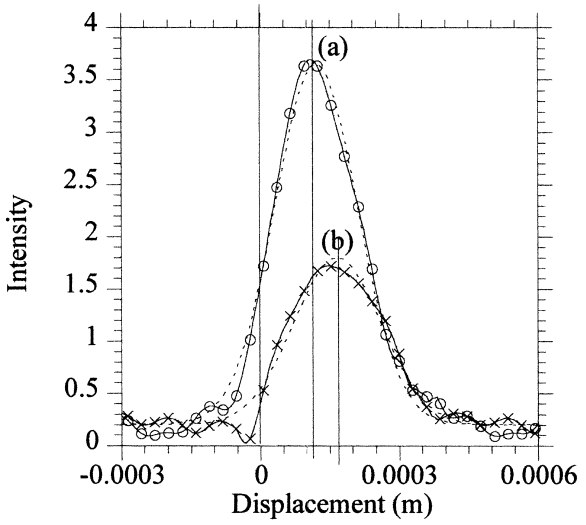

Fig. 5. Dynamic displacement profile extracted from dynamic NMR images of the SPE column A operating at a flow-rate of 1 ml min^{-1}. The two dynamic displacement profiles shown are taken from individual pixels, at the outer edge of the column (—×) where the velocity higher than average and from the middle of the column (—○) where the velocity is close to average. Fits of a gaussian distribution to the displacement profiles are shown with dashed lines (· · · · · ·).

Typical maps of velocity and apparent diffusion for a 1 mm thick cross-section through the 1 ml HiTrap™ column are shown in Fig. 6, along with a single pixel row extracted from the images. Maps of both velocity and apparent diffusion show strong edge effects, with a region of higher than average velocity and apparent diffusion, approximately 1 pixel wide (47 μm or approximately one particle diameter), at the column wall. There is also a region of lower than average velocity, 3–4 pixels wide (150 μm or approximately four to five particle diameters) adjacent to the high velocity annulus. The central region of the column, shows some slight heterogeneites, but is generally flat. Similar images were acquired at varying points along the length of the column. Both velocity and apparent diffusion maps show similar radial variations in velocity and apparent diffusion, regions of higher than average velocity have corresponding higher than average apparent diffusion coefficients. Fig. 6c shows that a plot of velocity versus distance, eliminating the data very close to the wall is a parabola with a velocity at the centre slightly higher than closer to the wall, as would be expected. The higher than average mobile phase velocity at the edge of the column is consistent with a lower packing density at the edge of the column due to the ordering of particles imposed by the wall. This result is consistent with the data recently reported by [22] who used dynamic NMR imaging to map the velocity and apparent diffusion in a column packed with impermeable polystyrene beads. They observed a decrease in velocity and apparently diffusion approximately three particle

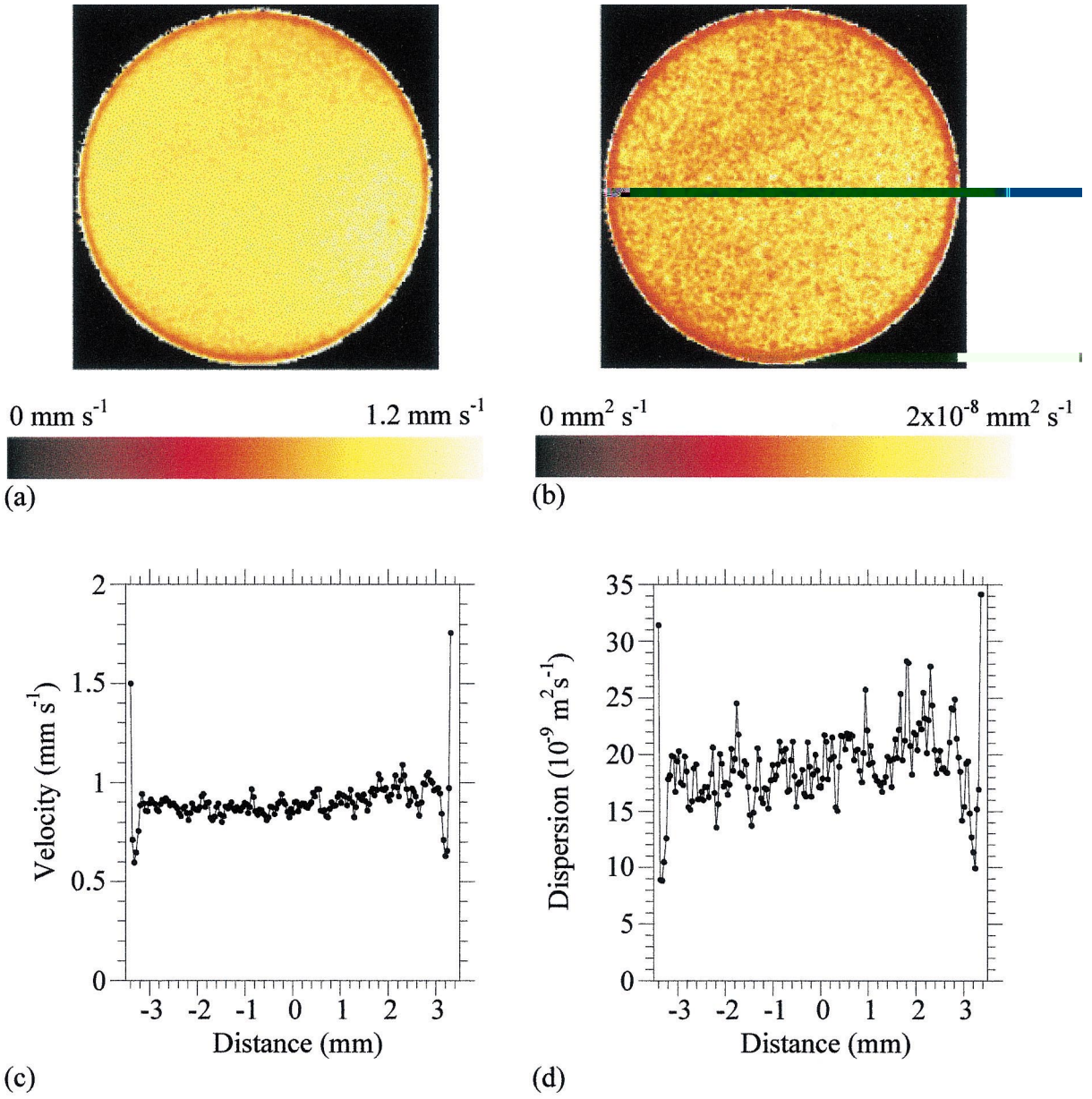

Fig. 6. Images of (a) axial velocity and (b) axial apparent diffusion for a horizontal cross section of the 1 ml HiTrap™ column operating at a flow-rate of 2 ml min^{-1}. The images shown represent a field of view of 7 mm. (c) Single pixel row extracted from the velocity image shown in (a) and (d) single pixel row extracted from the apparent diffusion map shown in (b).

diameters from the wall followed by a general increase in velocity and apparent diffusion as the wall was approached. The results reported in this present communication demonstrate that these same effects can also occur in columns packed with highly porous particles such as those used in chromatography applications. The distinctive variations at the wall reported in this work may also be compared to the dynamic NMR images of radial compressed chromatography columns previously reported [28,29]

for which no systematic radial variation in the flow behaviour was identified. The absence of radial variations in flow at the wall may be attributed to the radial compression stress or it may be a consequence of the courser resolution used in comparison to the particle diameter: The images reported by [28,29] on a column packed with spherical particles had a bead diameter to pixel size ratio of approximately 42 in comparison to the values of approximately 1 used in this current study. The other column studied by [28,29] had irregular shaped particles which again may mask such wall effects.

To illustrate the dependence of packing density on the spatial distribution of velocity and apparent diffusion dynamic NMR images of a horizontal cross-section of the three SPE columns studied operating at a flow-rate of 0.5 ml min^{-1} are shown in Fig. 7. Fig. 8 shows an extracted row from the velocity and apparent diffusion images shown in Fig. 7. Fig. 8 also shows the radial average velocity and apparent diffusion profiles calculated from the images shown in Fig. 7. The high velocity region at the column wall decreases with increasing packing density. The region of low velocity towards the edge of

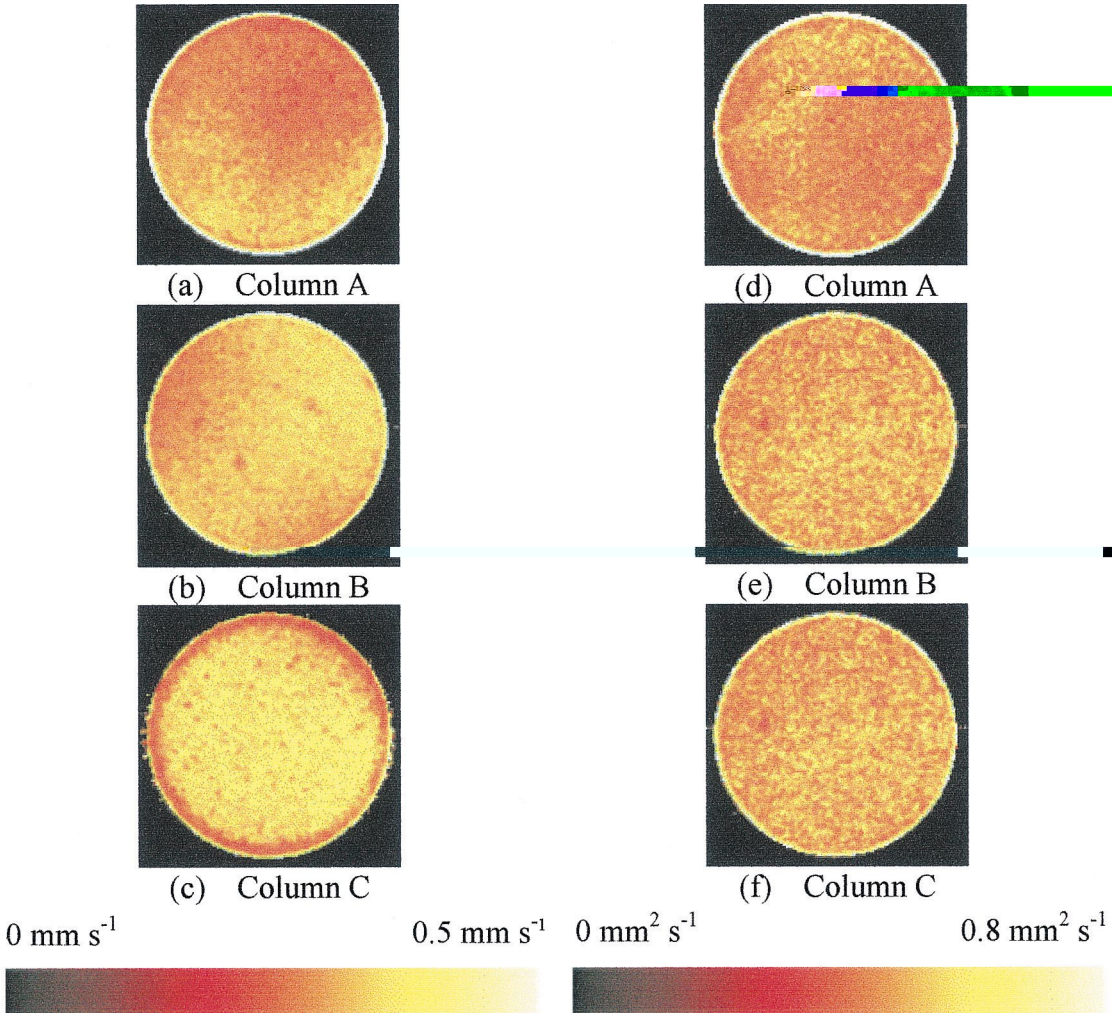

Fig. 7. Axial velocity images (a), (b) and (c) and axial apparent diffusion images (d), (e) and (f) of a horizontal cross section of SPE columns A, B and C respectively, operating at a flow-rate of 0.5 ml min^{-1}. The images shown represent a field of view of 6 mm.

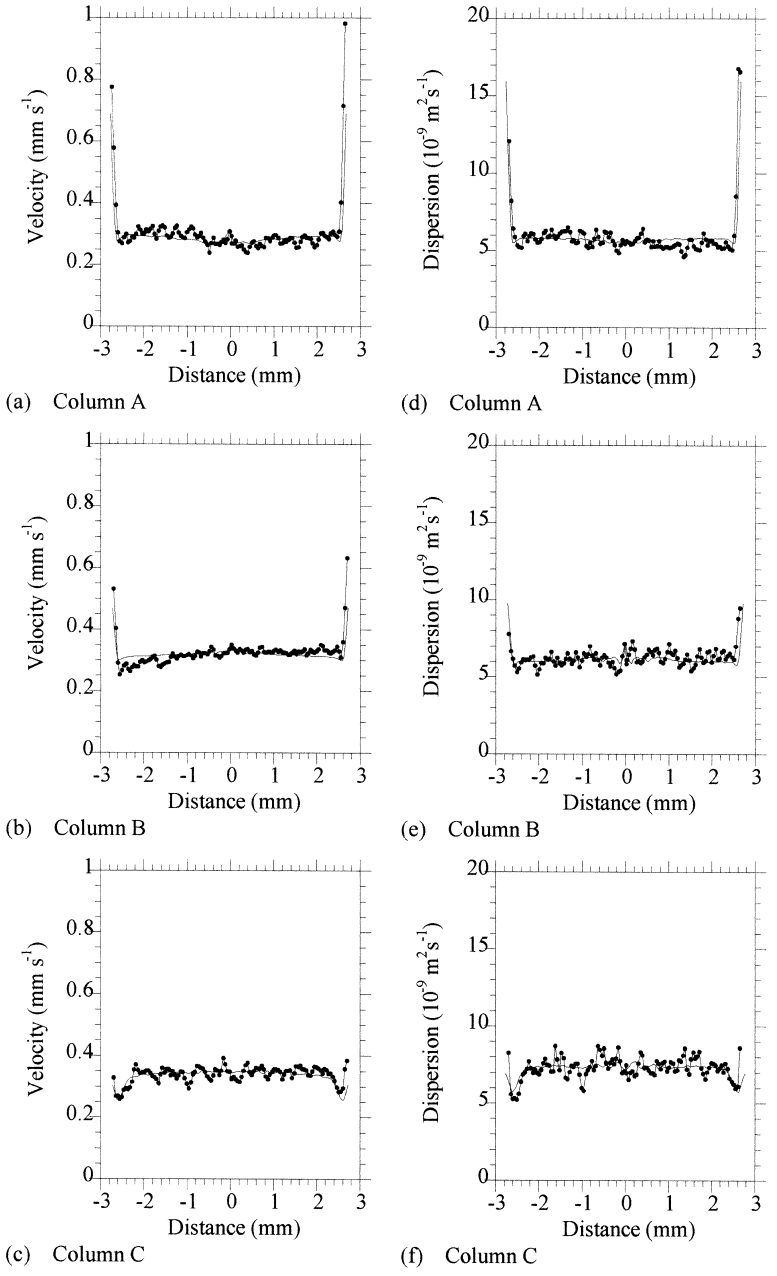

Fig. 8. Axial velocity profiles (a), (b) and (c) and axial apparent diffusion profiles (d), (e) and (f) of SPE columns A, B and C respectively showing a single pixel row (●) and the radial average value (—) extracted from the maps shown in Fig. 7.

the column starts to appear as the packing density is increased and is only significant for column C. These results show that the radial variations in velocity and dispersion are highly sensitive to the packing density of the column. This effect is probably explained by the physical nature of the agarose based Sepharose™ High Performance gel packing material. The gel particles would be easily deformed under mechanical

stress and thus the radial distribution of packing density would be altered.

The spatial heterogeneities in velocity observed by the dynamic NMR imaging measurements were quantified in terms of the variance in the velocity distribution over the column cross-section. For the SPE columns A, B and C operating at a flow-rate of 0.5 ml min^{-1} the variance in the velocity distribution was in the ratio 1: 0.3: 1.3 (A: B: C) for the three columns. This shows that in terms of minimising the band broadening resulting from spatial heterogeneities in the velocity distribution the column packed with the medium packing density appears to be most efficient.

Dynamic NMR images measured at flow-rates of 0.25, 0.5 and 1 ml min^{-1} for the same cross-section of column A showed the effect of higher than average solvent flow at the column wall at all flow-rates, and this effect became more significant with increasing flow-rate. Over the central region of the column cross-section examined there was some correlation between the flow velocities recorded at the three flow-rates studied. For example, the correlation coefficient between the velocity values over a central square region of length 3.2 mm for flow-rates of 0.25 ml min^{-1} and 1 ml min^{-1} was 0.82. Thus we see that even at this low packing density the structure of the bed that gives rise to heterogeneities in the flow velocity is maintained as the flow-rate is increased, a result that can be expected for a reasonably rigid structure.

4. Conclusions

From the NMR techniques employed in this work it has been possible to make an assessment of the column performance in terms of the reduced HETP and spatial variation in velocity and dispersion. All the measurements, by their very nature monitor the column performance over different length and time scales, and this is important to keep in mind when comparing the reduced HETP reported to the values measured by conventional chromatography techniques. The overall band broadening observed in the D_2O imaging experiments will be consistent with that observed in conventional techniques, however this method also allows us to observe the broadening of the band as it moved through the central region of the column — so separating the effects of the band broadening due to the column inlet and outlet. The PGSE measurements (acquired with no spatial resolution) describe the properties of the fluid flow averaged over a large section of the column. The reduced HETP determined from these measurements, h_{PGSE}, describes the effect of velocity fluctuations occurring over a time scale of 20–400 ms as the liquid moves in a volume equivalent to several particles. This experiment is therefore sensitive to the contribution of trans particle, trans channel flow fluctuations. The dynamic NMR imaging experiments measure the spatial variation in velocity and dispersion and are sensitive to the contribution to the overall HETP resulting from trans column velocity fluctuations. Images of the progression of the injection of D_2O through the column demonstrate the great importance of the column inlet on the overall band broadening observed.

NMR velocities and apparent diffusion maps of all the columns studied showed significant edge effects. The 1 ml HiTrap™ column showed a region of higher than average velocity and apparent diffusion, approximately 1 pixel wide (47 μm) — approximately one particle diameter, at the column wall. There was also a region of lower than average velocity and apparent diffusion 3–4 pixels wide (150 μm), adjacent to the high velocity region at the column wall. The central region of the column showed only slight heterogeneities in flow velocity. Similar radial variations have previously been observed by dynamic NMR imaging of flow through columns of impermeable particles [22], but have not previously been observed for porous chromatography gels [28,29]. The effect of column packing density on these edge effects was further investigated by comparing the dynamic NMR images of the three SPE columns prepared with varying packing densities. As the packing density was increased the high velocity and apparent diffusion region at the edge of the column decreased, however the low velocity and apparent diffusion region towards the edge of the column became more apparent. In terms of minimising the band broadening due to spatial heterogeneities in the

velocity distribution the column packed with the medium packing density appears to be most efficient.

5. Nomenclature

A	Numerical coefficient in the Knox equation
B	Numerical coefficient in the Knox equation
C	Numerical coefficient in the Knox equation
D	Numerical coefficient in the Knox equation
D_{app}	Apparent diffusion coefficient
D_{m}	Diffusion coefficient of the bulk liquid
d_p	Particle diameter
g	Gradient strength
g_{m}	Maximum gradient strength
H	Height equivalent to a theoretical plate (HETP)
H_{PGSE}	HETP determined from PGSE measurements
h	Reduced HETP
h_{PGSE}	Reduced HETP determined from PGSE measurements
h_a	Axial reduced HETP
h_t	Transverse reduced plate height
k_v	Peak position of gaussian distribution
k_{FWHM}	Full width half maximum of gaussian distribution
N	Number of data points in the dynamic displacement profile (after zero filling)
n	Numerical coefficients in the Knox equation
n_{D}	Number of velocity encoded images acquired
$\bar{P}_s$	Average probability distribution
$\boldsymbol{R}$	Dynamic displacement
S	NMR Signal intensity
$\boldsymbol{q}$	Wave vector describing gradient strength and duration
u	Cross-sectional average velocity of the inter particle fluid
$\bar{u}$	Velocity averaged over intra and inter particle fluid
v	Reduced velocity of the inter particle fluid
$\bar{v}$	Reduced velocity averaged over intra and inter particle fluid
z	Zone migration distance

Greek letters

Δ	Separation between magnetic field gradient pulses
δ	Gradient duration
σ^2	Zone variance
γ	Gyromagnetic ratio for protons

Acknowledgements

Sally G. Harding gratefully acknowledges Pharmacia & Upjohn for financial support. The authors are grateful to Rolf Hjorth and Lars Hagel for valuable comments on the manuscript.

References

[1] J.C. Giddings, Dynamics of Chromatography, Dekker, New York, 1965.
[2] G. Sofer, L. Hagel, Handbook of Process Chromatography — A Guide to Optimisation, Scale-up and Validation, Academic Press, London, 1997.
[3] G. Guiochon, T. Farkas, H. Guan-Sajonz, J. Koh, M. Sarker, B.J. Stanley, T. Yun, J. Chromatogr. A 762 (1997) 83.
[4] J.D. Seymour, P.T. Callaghan, AIChE J. 43 (1997) 2096.
[5] P.T. Callaghan, Principles of Nuclear Magnetic Resonance Microscopy, Clarendon Press, Oxford, 1991.
[6] U. Tallarek, E. Baumeister, K. Albert, E. Bayer, G. Guiochon, J. Chromatogr. A 696 (1995) 1.
[7] E. Bayer, E. Baumeister, U. Tallarek, K. Albert, G. Guiochon, J. Chromatogr. A 704 (1995) 37.
[8] L.D. Plante, P.M. Romano, E.J. Frenandez, Chem. Eng. Sci. 49 (1994) 2229.
[9] E.J. Ferandez, C.A. Grotegut, G.W. Braun, K.J. Kirschner, J.R. Staudaher, M.L. Dickson, V.L. Ferandez, Phys. Fluids 7 (1995) 468.
[10] G. Guillot, G. Kassab, J.P. Hulin, P. Rigord, J. Phys. D: Appl. Phys. 24 (1991) 763.
[11] S.N. Mitchell, L. Hagel, E.J. Fernandez, J. Chromatogr. A 779 (1997) 73.
[12] M. Ilg, J. Maier-Rosenkranz, W. Muller, K. Albert, E. Bayer, D. Höpfel, J. Magn. Reson. 96 (1992) 335.
[13] E.N. Lightfoot, A.M. Athalye, J.L. Coffman, D.K. Roper, T. W Root, J. Chromatogr. A 704 (1995) 45.

[14] U. Tallarek, K. Albert, E. Bayer, G. Guiochon, AIChE J. 42 (1996) 3014.
[15] U. Tallarek, E. Bayer, G. Guiochon, J. Am. Chem. Soc. 120 (1998) 1494.
[16] E. Baumeister, U. Klose, K. Albert, G. Guiochon, J. Chromatogr. A 694 (1995) 321.
[17] U. Tallarek, D. Van Dusschoten, H. Van As, G. Guichon, E. Bayer, Angew. Chem. Int. Edit. 37 (1998) 1882.
[18] U. Tallarek, D. Van Dusschoten, H. Van As, E. Bayer, G. Guichon, J. Phys. Chem. B 102 (1998) 3486.
[19] H. Van As, W. Palstra, U. Tallarek, D. Van Dusschoten, Mag. Res. Imag. 16 (5-6) (1998) 569.
[20] U. Tallarek, D. van Dusschoten, H. Van As, G. Guiochon, E. Bayer, Magn. Reson. Imaging 16 (5–6) (1998) 699.
[21] U. Tallarek, F.J. Vergeldt, H. Van As, J. Phys. Chem. B 103 (1999) 7654–7664.
[22] J. Park, S. Gibbs, AIChE J. 45 (1999) 655.
[23] Y.E. Kutsovsky, L.E. Scriven, H.T. Davis, B.E. Hammer, Phys. Fluids 8 (1996) 863.
[24] V. Rajanayagam, S.G. Yao, J.M. Pope, Magn. Reson. Imaging 13 (1995) 729.
[25] A. Feinauer, S.A. Altobelli, E. Fukushima, Magn. Reson. Imaging 15 (1997) 479.
[26] B. Manz, P. Alexander, L.F. Gladden, Phys. Fluids 11 (1999) 259.
[27] A.J. Sederman, M.L. Johns, P. Alexander, L.F. Gladden, Chem. Eng. Sci. 53 (1998) 2117.
[28] U. Tallarek, L.E. Bayer, D. Van Dusschoten, T. Scheenen, H. Van As, G. Guiochon, U.D. Neue, AIChE J. 44 (1998) 1962.
[29] D. Van Dusschoten, U. Tallarek, T. Scheenen, U.D. Neue, H. Van As, Magn. Reson. Imaging 16 (5–6) (1998) 703.
[30] L. Hagel, in: J.C. Janson, L. Rydén (Eds.), Protein Purification; Principles, High Resolution Methods and Applications, Wiley–VCH, New York, 1998, pp. 86–87, Ch. 3.
[31] R.A. Shalliker, B.S. Broyles, G. Guiochon, J. Chromatogr. A 826 (1998) 1.
[32] B.S. Broyles, R.A. Shalliker, G. Guiochon, J. Chromatogr. A 835 (1999) 367.
[33] R.A. Shalliker, B.S. Broyles, G. Guiochon, J. Chromatogr. A 865 (1999) 83.
[34] B.S. Broyles, R.A. Shalliker, G. Guiochon, J. Chromatogr. A 867 (2000) 71.
[35] R.A. Shalliker, B.S. Broyles, G. Guiochon, Anal. Chem. 72 (2000) 323.